


RESEARCH PAPER



Synthesis and biological evaluation of thiazolidinedione derivatives with high ligand efficiency to *P. aeruginosa* PhzS

Thamires Quadros Froes^{a*}, Bianca Trindade Chaves^{b*}, Marina Sena Mendes^b, Rafael Matos Ximenes^c, Ivanildo Manguiera da Silva^c, Priscila Brandão Gomes da Silva^c, Julianna Ferreira Cavalcanti de Albuquerque^c and Marcelo Santos Castilho^{a,b,d} 

^aPrograma de Pós-graduação em biotecnologia da, Universidade Estadual de Feira de Santana, Feira de Santana, Brazil; ^bFaculdade de Farmácia da, Universidade Federal da Bahia, Salvador, Brazil; ^cDepartamento de Antibióticos da, Universidade Federal de Pernambuco. Av. Prof. Moraes Rego, Recife-Pe, Brazil; ^dPrograma de Pós-Graduação em Farmácia da, Universidade Federal da Bahia, Salvador, Brazil

ABSTRACT

The thiazolidinone ring is found in compounds that have wide biological activity and there is mechanism-based evidence that compounds bearing this moiety inhibit *P. aeruginosa* PhzS (*PaPzS*), a key enzyme in the biosynthesis of the virulence factor named pyocyanin. Ten novel thiazolidinone derivatives were synthesised and screened against *PaPzS*, using two orthogonal assays. The biological results provided by these and 28 other compounds, whose synthesis had been described, suggest that the dihydroquinazoline ring, found in the previous hit (**A**- K_d = 18 μM and LE = 0.20), is not required for *PaPzS* inhibition, but unsubstituted nitrogen at the thiazolidinone ring is. The molecular simplification approach, pursued in this work, afforded an optimised lead compound (**13**- 5-(2,4-dimethoxyphenyl)thiazolidine-2,4-dione) with 10-fold improvement in affinity (K_d = 1.68 μM) and more than 100% increase in LE (0.45), which follows the same inhibition mode as the original hit compound (competitive to NADH).

EXECUTIVE SUMMARY

- PhzS is a key enzyme in the pyocyanin biosynthesis pathway in *P. aeruginosa*.
- Orthogonal assays (TSA and FITC) show that fragment-like thiazolidinedione derivatives bind to *PaPzS* with one-digit micromolar affinity.
- Fragment-like thiazolidinedione derivatives bind to the cofactor (NADH) binding site in *PaPzS*.
- The molecular simplification optimised the ligand efficiency and affinity of the lead compound.

ARTICLE HISTORY

Received 8 January 2021
Revised 29 April 2021
Accepted 11 May 2021

KEYWORDS





Thiazolidinone; pyocyanin biosynthesis inhibition; *P. aeruginosa*; antimicrobial resistance

Introduction


Compounds bearing the 4-thiazolidinone, 2,4-thiazolidinedione, rhodanine (2-thioxo-4-thiazolidinone) moieties have been explored by medicinal chemists since the 1960s^{1,2}. In fact, many authors claim that 4-thiazolidinone ring might be considered a privileged scaffold for drug design efforts^{3,4}. One of the main achievements that have fuelled the drug design efforts with 4-thiazolidinone derivatives was the introduction of antidiabetic drugs to the market (i.e. peroxisome proliferator-activated receptor-γ (PPAR) agonists⁵ and aldose reductase inhibitors⁶). However, this class of compounds has also shown promise in several fields (Figure 1). For instance, 5-arylidene-2,4-thiazolidinone derivatives are low micromolar inhibitors of Pteridine reductase 1 from *Leishmania major*⁷ that are also active against *L. braziliensis* and *L. infantum* promastigotes⁸, and benzylidene-2,4-thiazolidinedione derivatives⁹ and thiazolidine-2,4-diones derivatives with a carboxylic ester substituent at N-3¹⁰ have shown activity against protein-tyrosine phosphatase 1B (PTP1B). More recently, Froes and co-workers

included the inhibition of *P. aeruginosa* PhzS to the list of biological activities ascribed to compounds bearing the 2,4-thiazolidinedione ring and underscored that these compounds might be employed to battle resistant bacteria¹¹.

Antimicrobial resistance (AMR) causes more than 700,000 deaths each year¹² and burdens approximately 2 million patients in the USA¹³. To make matters worse, these figures may escalate to 10 million deaths per year if no action is taken¹⁴. Nevertheless, the investment in the development of novel antibiotics has been steadily decreasing^{15,16}. The roots for this problem have already been discussed, but most of them are somehow related to the fact that both bactericidal and bacteriostatic drugs are responsible for an evolutionary pressure that selects resistant strains¹⁷. In order to overcome this dilemma, antivirulence drugs, which aim at 'disarming' the pathogens instead of killing them, have been pursued^{18–21}. In contrast to previous studies that focus on quorum sensing modulation^{22–25}, in this work we target enzymes from the pyocyanin (PYO) biosynthesis pathway in *P. aeruginosa*, a Gram-negative bacillus with high degree of resistance to available

CONTACT Marcelo Santos Castilho  castilho@ufba.br  Faculdade de Farmácia, Universidade Federal da Bahia, CEP 40.140-115, Salvador, Bahia, Brazil. Julianna Ferreira Cavalcanti de Albuquerque  julianna@ufpe.br  Departamento de Antibióticos da, Universidade Federal de Pernambuco, Av Professor Moraes Rego, 1235, CEP 50.670-901, Recife-Pernambuco, Brazil

*Equal contribution to the work.

 Supplemental data for this article can be accessed [here](#).

© 2021 The Author(s). Published by Informa UK Limited, trading as Taylor & Francis Group.

This is an Open Access article distributed under the terms of the Creative Commons Attribution License (<http://creativecommons.org/licenses/by/4.0/>), which permits unrestricted use, distribution, and reproduction in any medium, provided the original work is properly cited.

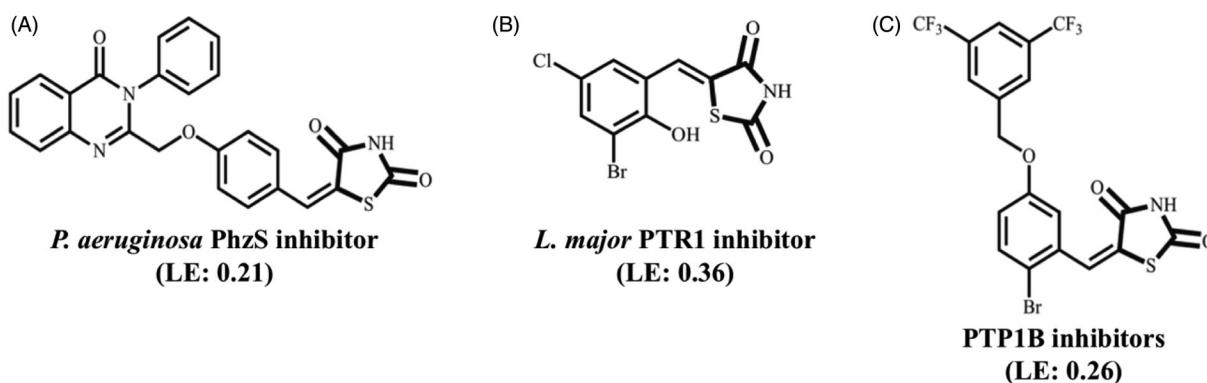


Figure 1. Biological activity of selected 4-thiazolidinone derivatives.

drugs²⁶, in particular PhzS, an enzyme that catalyses the last step of the PYO biosynthesis, because A) genetic validation (*phzS* gene knockout) suggests that this protein is crucial for *P. aeruginosa* infection progression²⁷; B) *in silico* tools predict this target to be druggable²⁸; C) the reaction catalysed by PhzS is NADH-dependent^{29,30}. This last feature prompted the analysis of thiazolidine-2,4-dione derivatives that might mimic the interaction profile of the purine ring from NADH. These efforts already led to the identification of (E)-5-(4-((4-oxo-3-phenyl-3,4-dihydroquinazolin-2-yl)methoxy)benzylidene)thiazolidine-2,4-dione (**A**) as a low micromolar affinity ($K_d = 18 \mu\text{M}$) inhibitor of PhzS from *P. aeruginosa*¹¹. If one compares the ligand efficiency (LE) of this compound (0.21) to the LE of other thiazolidine-2,4-dione derivatives that display a similar competitive mechanism to NADPH (i.e. **B**- LE = 0.36), it becomes clear that the initial hit should have poor complementarity to its binding site. In order to identify the moieties that are essential for PhzS inhibition, molecular modification strategies, such as replacement of dihydroquinazoline moiety by lipophilic, less-bulky substituents, the addition of aromatic rings at the nitrogen from the thiazolidine-2,4-dione ring, etc. were carried out. The biological profile of those compounds shows that dihydroquinazoline moiety is detrimental to LE and that N-substitution is not compatible with *Pa*PhzS binding. Moreover, the most promising lead compound reported in this work not only has improved affinity to its target ($K_d = 1.68 \mu\text{M}$) and increased LE (0.45) but also follows the same mode of inhibition of the previous hit (competition with NAD⁺).

Materials and methods

The reagents were purchased from Sigma-Aldrich and the solvents from the Vetec and Dinâmica brands. The reactions were monitored by thin-layer chromatography (TLC) using Merck Silica gel 60 F254 chromatographic plates, 0.25 mm thick, observed under ultraviolet light of two different wavelengths (254 or 366 nm).

The reactions were carried out in an oil bath with Fisatom model 752 A hot plate with magnetic stirring. The solvents were evaporated under reduced pressure using a Fisatom rotary evaporator, model 550. The melting points were measured in capillaries using a Quimis fusiometer, model 340.23, and are uncorrected. The products were weighed on a Bel analytical balance, model Mark 210 A and dried in a Liobras freeze dryer, L101.

All compounds were characterised by NMR ¹H, NMR ¹³C, and DEPT analyzes. The NMR ¹H and NMR ¹³C spectra were obtained on Varian instruments, model Unity Plus (400 MHz for ¹H; 100 MHz for ¹³C) or Bruker AMX (300 MHz for ¹H and 75.5 MHz for ¹³C), using tetramethylsilane as an internal standard. The multiplicity of

signals in the NMR ¹H spectra were designated as follows: s (singlet); d (doublet); t (triplet); dd (double doublet); q (quartet); or m (multiplet). The IR spectra were obtained using an Infra-red Absorption Spectrophotometer – FTIR Bruker Model IFS 66 or Perkin Elmer – Spectrum 400 using KBr tablets. For high-resolution mass spectra (HRMS), the electrospray (ESI) ionisation technique was used in positive (ESI⁺) or negative (ESI⁻) modes with time-of-flight (TOF) detection, measured on a Shimadzu LC-ESI-qTOF-MS device.

Chemistry

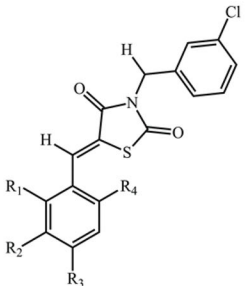
Thiazolidine-2,4-dione derivatives (**1** – **38** - Tables 1 and 2) were obtained by well-established synthetic routes based on Knoevenagel condensation. Compounds **2**³¹, **4**³², **5**^{33,34}, **8**–**9**⁷, **10**³⁵, **11**–**17**⁷, **18**³⁶, **19**⁸, **22**^{37,38}, **23**³⁹, **24**^{35,40}, **25**^{37,41,42}, **26**⁴³, **27**^{43,44}, **29**⁴⁵, **30**⁴⁶, **31**^{3,47}, **32**⁴⁸, **33**⁸, **35**³⁶, **37**^{33,49} (Supplementary material) were synthesised according to previously published protocols, whereas novel compounds were synthesised through the general steps described in Figure 2.

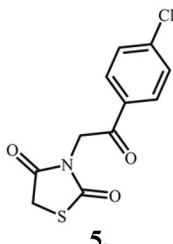
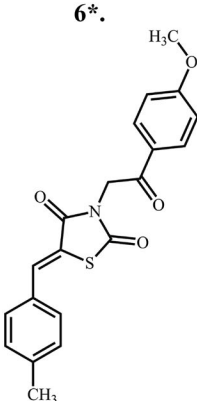
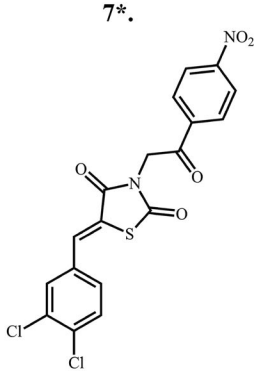
The starting compound (thiazolidine-2,4-dione) was obtained as described by Libermann and Himbert (1948)⁵⁰, with the modifications proposed by Albuquerque et al. (1995)⁵¹. This reaction occurs by condensation of monochloroacetic acid and thiourea in an aqueous medium under reflux for 24 h. Molecular formula C₃H₃O₂NS; yield 78%; mp 118–120 °C; *R*_f 0.48 (0.9:0.1 CHCl₃/MeOH). Recrystallization: water.

General synthesis of novel N-substituted 5-benzylidene-thiazolidine-2,4-dione derivatives (**1**, **3**, **6** and **7**)

Compounds **1**, **3**, **6** and **7** were synthesised in two steps. First, a solution of KOH dissolved in methanol was added drop-wise, under constant stirring, to thiazolidine-2,4-dione solubilised in 10 ml of methanol (1:1 molar ratio). After 15 min, under magnetic stirring, the appropriate phenacyl bromide was added drop-wise to the reaction mixture, which was kept under reflux for 24 h. After that, the reaction product was filtered and washed with ice-cold ethanol. In the second step, the product obtained in the previous step was dissolved in methanol and two drops of piperidine. After 10 min, equimolar amounts of the appropriate aromatic benzaldehyde were added to the flask, which was kept at 75 °C, under magnetic stirring and reflux for 8 h. Then, the product was filtered and washed with ice-cold ethanol, crystallised, and dried in an oven at 40 °C.

Table 1. N-substituted 5-arylidene-thiazolidine-2,4-dione derivatives assayed against *PaPhzS*.

	Numbe	R ₁	R ₂	R ₃	R ₄
	r				
1*	H	Cl	H	OH	
2	H	NO ₂	H	H	
3*	Cl	H	H	Cl	
4	H	H	OCH ₃	H	

 <p>5.</p>	 <p>6*.</p>	 <p>7*.</p>
--	---	--

*Novel compounds.

1. (Z)-5-(5-chloro-2-hydroxybenzylidene)-3-(3-chlorobenzyl)thiazolidine-2,4-dione. Chemical formula: C₁₇H₁₁Cl₂NO₃S; MW 378.9837; *mz* 378.9837 (100%); Yield: 55%; MP 201–202 °C; *R_f* 0.55 (CHCl₃:MeOH; 9.6:0.4). Infra-red (KBr, cm⁻¹ 1716 (C=O₄); 1676 (C=O₂); 1605 (C=C). NMR ¹H (300 MHz, CDCl₃) (δppm): 5.51 s 2H, CH₂ 8.21; 5.36 (s 1H OH); 8.22 s 1H C=H; 6.83 (d 1H *J*=7.5) 7.19 (d 1H *J*=7.45) 7.14 (s 1H Ar) Benzylidene. 7.44 (s 1H Ar); 7.29 (ddd 1H, H₄ *J*=7.10; 1.5; 1.5) Ar; 7.12 (ddd *J*=7.5, 1.5, 1.5) Ar, benzyl. NMR ¹³C (CDCl₃) (DEPT MHz): δ ppm: 171.51 (C=O₂); 163.3 (C=O₄) 116.00 C=C; 143.79 C=H, 47.1 CH₂; 144.58; 135.01; 133.12; 127.21; 126.11; 132.21 (benzyl). 154.3, 131.2; 128.2; 127.1; 119.1; 118.1 (benzylidene) HRMS⁺, 378.9837 (100%) calculated, 378.9828.

3. (Z)-3-(3-chlorobenzyl)-5-(2,6-dichlorobenzylidene)thiazolidine-2,4-dione. Chemical formula: C₁₇H₁₀Cl₃NO₂S; MW 396.9498; *mz* 396.9498 (100%); Yield: 57%; MP 110–111 °C; *R_f* 0.47 (Hex:CHCl₃, 0.7:0.3). Infra-red (KBr, cm⁻¹): (C=C) 1743 (C=O₄), 1673 (C=O₂); 1610 (C=C). NMR ¹H (300 MHz, CDCl₃) (δppm): 5.56 (s 2H (CH₂); 8.21 s 1H; CH=); 7.52 (dd H₃-H₅ *J*=7.5, 1.5) benzylidene); 7.12 (ddd H₃-H₆ *J*=7.57, 1.50, 1.45). 7.28 (dd 1H, *J*=7.51, 1.48) Ar; 7.30 (dd 1H, *J*=7.50, 1.50) Ar, benzyl. NMR ¹³C (CDCl₃) (DEPT (75.4 MHz): δppm: 172.9.1. (C=O₂); 163.7.21 (C=O₄) 115.41 C=C; 146.81 C=H; (143.13; 131.8; 131.21; 133.3; 135.36; 126.65; benzyl). 136.73; 131.63; 129.87; 126.55; 127.53; 132.73, benzylidene). HRMS⁺ 396.9498 (100%) calculated, 396.8989 found.

6. (Z)-3-(2-(4-methoxyphenyl)-2-oxoethyl)-5-(4-methylbenzylidene)thiazolidine-2,4-dione. Chemical formula: C₂₀H₁₇NO₄S; MW. 367.0878; *mz* 367.0878 (100%) Yield: 78%; MP 174–176 °C; *R_f* 0.49 (Hex:EtOAc, 0.52:0.48). Infra-red (KBr, cm⁻¹ 1746 (C=O₄), 1676 (C=O₂); 1610 (C=C). NMR ¹H (300 MHz, CDCl₃) (δppm): 7.96 (s 1H, CH=); 6.13 s 2H (CH₂). 3.85 (s 3H, OCH₃); 2.37 s 3H

(CH₃); 7.61 (d H₂-H₆ *J*=7.30, 1.5) Ar; 7.20 (d H₃-H₅ (*J*=7.26, 1.5) Ar; (benzylidene). 7.87 (d H₂-H₆ (*J*=7.26, 1.5) Ar) (benzyl). NMR ¹³C (CDCl₃) (DEPT (75.4 MHz): δ ppm: 55.96, CH₃; 55.71 CH₂; 197.12 C=O; 174.73 (C=O); 167.3 C=O; 117 C=CH; 145.71 C=CH; 21.45 CH₃; 168.09; 114.33 × 2; 132.3 × 2; 129.9 (Ar); 134.8; 129.3 × 2; 128.7 × 2; 138.9 Ar. HRMS⁺, (367.0878 (100%) calculated, 367.0873 (100%) found.

7. (Z)-5-(3,4-dichlorobenzylidene)-3-(2-(4-nitrophenyl)thiazolidine-2,4-dione). Chemical formula: C₁₈H₁₀Cl₂N₂O₅S; MW. 367.4183; *mz* 367.0878 (100%); Yield: 78%; MP 230–231 °C; *R_f* 0.49 (CHCl₃:Hex, 0.8:0.2). Infrared (KBr, cm⁻¹ 1749 (C=O₄), 1678 (C=O₂); 1615 (C=C). NMR ¹H (300 MHz, CDCl₃) (δppm): 5.88 (s 2H CH₂); 8.33 (d 1H *J*=7.12), 8.38 (d 1H, *J*=7.15); 7.97 s 1H C=H; 7.57 (d 1H *J*=7.52) Ar; 7.41 d 1H *J*=7.51) Ar 7.22 (s 1H Ar). NMR ¹³C (CDCl₃) (DEPT (75.4 MHz): δ ppm: 55.15 (CH₂), 194.7 (C=O). 171.81 (C=O₂); 163.33 (C=O₄); 115.61 C=C; (127.98, 121.7, 153.02, 127.98, 121.7, 140.87) Ar (133.61; 126.7; 128.41; 131.81; 133.15) Ar. HRMS⁺, 367.0878 calculated, 367.0715 found.

General synthetic steps for novel 5-arylidene-thiazolidine-2,4-dione derivatives (7, 19–21, 28, 33–34, 36, 38)

Method: In a round bottom flask, 0.100 g (0.85 mmol) of Thiazolidine-2,4-dione (Ju-32) and 4 ml of ethanol were mixed, with stirring, until the complete solubilisation. Then, 2 drops of piperidine were added. The mixture was kept under magnetic stirring at room temperature for 10 min. After this time, 0.17 g (0.85 mmol) of benzaldehyde was added. The flask was kept at 75 °C, under magnetic stirring and reflux for 5–15 h, depending on each aldehyde. After cooling the solvent, the product was filtered through ice-cold ethanol.

Table 2. 5-arylidene-thiazolidine-2,4-dione derivatives assayed against *PaPhzS*.

	R₁	R₂	R₃	R₄	R₅
	8	Cl	H	Cl	H
9	H	Cl	Cl	H	H
10	H	H	Cl	H	H
11	H	H	Br	H	H
12	H	OCH ₃	OH	H	H
13	OCH ₃	H	OCH ₃	H	H
14	Br	H	H	H	F
15	OH	Br	H	Cl	H
16	OH	H	H	Cl	H
17	Cl	H	H	H	Cl
18	NO ₂	H	H	H	H
19	Cl	Cl	H	Cl	H
20*	Br	OH	OCH ₃	H	H
21*	H	Br	CH ₃	H	H
22	H	OH	H	H	H
23	H	OCH ₃	OCH ₃	H	H
24	H	H	CH ₃	H	H
25	H	OCH ₃	OCH ₃	OCH ₃	H
26	H	CH ₂ OCH ₃	H	H	H
27	H	H	CH ₂ OCH ₃	H	H
28*	OCH ₃	H	OCH ₃	OCH ₃	H

29 	30 	31 	32 	33
34* 	35* 	36 	37 	38*

*Novel compounds.

20. (*Z*)-5-(2-bromo-3-hydroxy-4-methoxybenzylidene)thiazolidine-2,4-dione. Chemical formula: C₁₁H₈BrNO₄S; MW 328.9357; *mz* 328.9357 (100%). Yield: 59%; MP 245 °C *R_f*. 0.51 (0.9:0.1 (CHCl₃: MeOH). Infra-red (KBr, cm⁻¹): 1746 (C=O₄), 1676 (C=O₂); 1610 (C=C). NMR ¹H (300 MHz, CDCl₃ 300 MHz (δ ppm): 13.12 (s 1H (NH)); 8.21 (s 1H, CH=); 6.73 (d 1H, H₅, *J*=7.48); 3.81 (s 3H, CH₃) 5.37 (s 1H, OH). NMR ¹³C (CDCl₃) (DEPT (75.4 MHz): δ ppm: 167.5. (C=O₂); 166.27 (C=O₄); 117.01 C=C; 142.58 CH=; (Ar 130.01; 115.31; 142.15; 153.18; 111.32; 123.01). HRMS⁺, (328.9357 (100%) calculated, 328.9348 (100%) found.

21. (*Z*)-5-(3-bromo-4-methylbenzylidene)thiazolidine-2,4-dione. Chemical formula: C₁₁H₈BrNO₂S; MW 296.9459; *mz* 296.9459

(100%); Yield: 61%; MP 196–197 °C. *R_f* 0.50 (8.5:1.5 Hex. AcOEt). Infra-red (KBr, cm⁻¹): 1745 (C=O), 1673 (C=O); 1610 (C=C). NMR ¹H (300 MHz, DMSO-d₆): (δ ppm) 12.89 NH (amide), 7.94, s 1H CH=; 7.47 s 1H₂; 7.10, d 1H₅ *J*=7.43 Ar) 7.55 dd 1H₆ *J*=7.5, 1.48; 2.37 s 3H (CH₃). NMR ¹³C (DEPT (75.5 MHz, DMSO-d₆): (δ ppm) 166.92 (C=O); 167.0 (C=O); 115.98 C=C; 143.23 CH=; (133.97, 129.87, 124.11; 137.17; 130.81; 128.01 Ar); 23.91 (CH₃). HRMS⁺, 296.9459 (100%) calculated 296.9145 found.

28. (*Z*)-5-(2,4,5-trimethoxybenzylidene)thiazolidine-2,4-dione. Chemical formula: C₁₃H₁₃NO₅S; MW 295.0419; *mz* 295.0514 (100%); Yield: 67%; MP. 158–160 °C *R_f*. 0.52 (0.83:0.17 Hex; AcOEt). Infra-red (KBr, cm⁻¹): 1747 (C=O₄), 1651 (C=O₂); 1611 (C=C). NMR ¹H

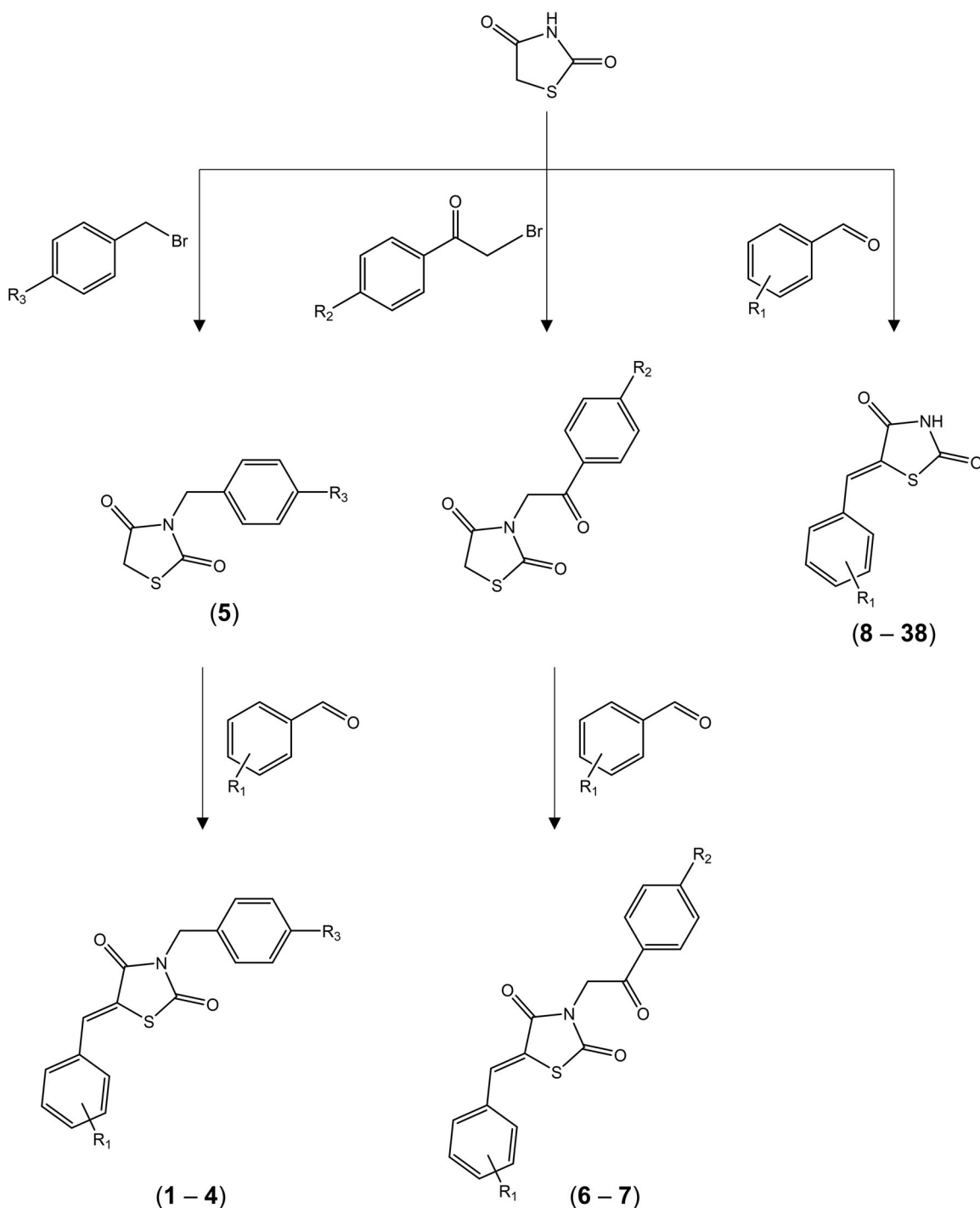


Figure 2. General synthesis steps to obtain 2,4-thiazolidinedione derivatives.

(300 MHz, CDCl_3 300 MHz (δ ppm): 12.76 (s 1H NH); 8.21 (s 1H, CH=); 3.84 (s 3 OCH₃, ortho, meta, para Ar) 6.43 (s 1H CH meta) 6.70 (s 1H CH para). NMR ¹³C (CDCl_3) (DEPT (75.4 MHz): δ ppm: 166.9 (C=O₂); 166.35 (C=O₄) 116.31 C=C; 143.57 CH=; 55.91 \times 3 CH₃. 108.5; 136.1; 99.31; 151.19; 142.51; 111.02 CH, Ar). HRMS⁺, 295.0514 (100%) calculated, 295.0413 found.

34. (Z)-5-(isoquinolin-4-ylmethylene)thiazolidin-2,4-dione. Chemical formula: C₁₃H₈N₂O₂S; MW 256.2798; m/z 256.0306 (100%); Yield: 77%; MP 118–119.5 °C. R_f. 0.51 (0.99:0.01 MeOH:CHCl₃). Infra-red (KBr, cm⁻¹), 1623 (C=C), NMR ¹H (300 MHz, CDCl_3 300 MHz

(δ ppm): 12.32 (s 1H (NH)); 11.12 (s 1H NH); 7.97; (s 1H, CH=); 7.87 (s 1H, CH); 7.15; (d 1H) d Ar; 7.15 (dd, 1H (J=7.1; 1.5)) Ar; 6.98 (dd 1H, J=7.51; 1.5). 7.27 (dd 1H J=7.1; 1.5). 7.68 dd J=7.51. 1.50 Ar). NMR ¹³C (CDCl_3) (DEPT (75.4 MHz): δ ppm: 166.81 (C=O₂); 165.27 (C=O₄) 121.11 C=C; 142.8 CH=; (137.26; 112.8; 121.93; 120.03; 120.73; 119.87; 128.07 Ar) HRMS⁺, 256.2798 (100%) calculated, 256.0235 found.

36. (Z)-5-((2-hydroxynaphthalen-1-yl)methylene)thiazolidin-2,4-dione. Chemical formula: C₁₄H₉NO₃S; MW 271.0303; m/z 271.0303. (100%); Yield: 69%; MP 194–195 °C; R_f. 0.49 (0.96:0.04,

CHCl₃:MeOH). Infra-red (KBr, cm⁻¹): 1754 (C=O₄), 1676 (C=O₂); 1615 (C=C). NMR ¹H (300 MHz, CDCl₃ 300 MHz) (δ ppm): 12.32 (s 1H (NH)); 8.21 (s 1H, CH=); 5.37 (s 1H, OH); 7.78 (dd CH *J* = 7.1, 1.5); 7.52 (dd, H₁, H₃) *J* = 7.59; 1.5). 7.43 (dd *J* = 7.2, 1.5). 7.42 (dd *J* = 7.4, 1.51); 7.42, (dd *J* = 7.4, 1.51); 8.01 dd (*J* = 7.1; 1.5). 7.76 (d 1H, (*J* = 7.1); 6.97 (d 1H, *J* = 7.0). NMR ¹³C (CDCl₃) (DEPT (75.4 MHz): δ ppm: 167.51 (C=O₂); 166.38 (C=O₄) 117.06 C=C; 143.79 CH=; 155.3 C-OH; 120.0; 130.0 128.4; 130.1; 127.5, 123.5; 127.0; 122.8 128.7 Ar.). HRMS⁺, 271.0303 (100%). Calculated, 271.0299 found.

38. (Z)-5-((E)-3-(2-nitrophenyl)allylidene)thiazolidine-2,4-dione. Chemical formula: C₁₂H₈N₂O₄S; MW 276.2679. *mz* 276.0205. (100%); Yield: 69%; MP 119–120 °C. *R_f*. 0.52 (0.86:0.14 Hex; AcOEt). Infra-red (KBr, cm⁻¹): 1746 (C=O₄), 1677 (C=O₂); 1612 (C=C). NMR ¹H (300 MHz, CDCl₃) (δ ppm): 13.24 (s 1H (NH)); 7.97 (s 1H, CH=); 6.89 (d 1H, CH=) 7.39 (d 1H CH=) (8.01 dd 1H, *J* = 7.5, *J* = 1.5, Ar) (7.82 dd *J* = 7.5; *J* = 1.5), 7.91 (ddd 1H *J* = 7.5, 1.5, Ar); 7.89 (dd; 2H *J* = 7.0; 1.5 Ar). NMR ¹³C (CDCl₃) (DEPT (75.4 MHz): δ ppm: 168.12 (C=O₂); 167.91 (C=O₄) 119.07 C=C; 136; 126.04, 47.9; 124.01; 123.90; 129.01; 135.60; 127.28 HRMS⁺, 276.0205 (100%) calculated, 276.0201 found.

Biological methods

Expression and purification enzymes

The expression and purification of the PhzS from *P. aeruginosa* was performed as described by Greenhagen and co-workers²⁹ with minor modifications to improve the overall yield¹¹. Briefly, *E. coli* Rosetta (DE3) cells, containing the pET28a plasmid that codes for PhzS from *P. aeruginosa*, were grown at 37 °C (180 RPM), in LB medium supplemented with kanamycin (30 µg/mL) and chloramphenicol (34 µg/mL), until the OD₆₀₀ reached 0.6–0.8. Then, Isopropyl-b-D-thiogalactoside (IPTG) was added to the culture (final concentration 250 µM) and the temperature was reduced to 18 °C. After 24 h, the cells were harvested by centrifugation (100,000 RPM, Avanti J-E centrifuge (Beckman Coulter), 4 °C, 30 min) and resuspended in Potassium Phosphate buffer (50 mM) pH 8.0, supplemented with 300 mM NaCl and 1 mM phenylmethanesulphonyl fluoride (PMSF). Next, the cells were disrupted by sonication (10–15 s bursts with 30 s intervals between each burst, 8 Watts) in an ice bath. The soluble fraction was clarified by centrifugation (16000 rpm, 20 min, 4 °C) and then loaded onto a HisTrap HP column (GE Healthcare), pre-equilibrated with buffer A (Potassium Phosphate 50 mM (pH 8.0), NaCl (300 mM) and imidazole (20 mM)). The column was washed with 20 column volumes (CV) of buffer A and then with increasing concentrations of imidazole (50–500 mM) added to buffer A. All purification steps were followed by SDS-PAGE 12% and the final protein concentration was evaluated by measuring the UV/vis absorbance at 280 nm (theoretical extinction coefficient of 1.352 M⁻¹ cm⁻¹ according to ProtParam server, available in (<http://web.expasy.org/protparam/>)). The purified protein was stored in 30% glycerol at –80 °C until use.

Screening of thiazolidinedione derivatives by thermal shift assay (TSA)

TSA assays were performed on Applied Biosystems 7500 RT-PCR (Applied Biosystems, Foster City, CA USA), fitted with custom filter sets. All assays were carried out in triplicate on a 96-well PCR plate (PCR plates 96 well BioRad[®]), manually sealed with transparent capping strips (Flatcap strips BioRad[®]). The plates were

centrifuged for 2 min, 2000 rpm, at 25 °C and then the fluorescence of SYPRO[™] orange (S6650) was monitored (excitation wavelength = 492 nm and emission wavelength = 610 nm), while the plate was heated from 25 to 85 °C, in increments of 1 °C per minute.

The TSA conditions employed in this work were previously optimised¹⁶. Briefly, 5 µl of *PaPhzS* (5 µM final concentration), 1 µl of SYPRO[™] orange (5X), 13 µl of assay buffer (50 mM potassium phosphate, 300 mM NaCl, pH 8), and 1 µl DMSO (5% v/v), as a negative control, or the putative inhibitor (diluted in DMSO) were added to each well. All experiments were carried out in triplicate.

Raw fluorescence data were recorded within the Applied Biosystems 7500 Software v2.0, and then exported to NAMI⁵² for Tm calculation by the first-derivative method. Differences between Tm values (ΔTm) were considered statistically significant when *p* < .01, according to the One-way ANOVA followed by Dunnett's post-test for multiple comparisons, available in GraphPad Prism 8.0 software (GraphPad[®] Software, San Diego, CA, USA, www.graphpad.com).

Mode of inhibition by TSA

The mode of inhibition (competitive, non-competitive, uncompetitive) was evaluated by comparison to the thermal signatures described by Lea and co-workers⁵³. Hence, the ΔTm due to different concentrations of each thiazolidinedione derivative was employed to build sigmoid dose-response curves (APO-Tm curves), using non-linear regression (three parameters), available in GraphPad Prism 8.0 software (GraphPad[®] Software, San Diego, CA, USA, www.graphpad.com) (Equation (1)).

$$Y = Bottom + (Top - Bottom) / (1 + 10^{(LogEC50 - X)}) \quad (1)$$

where *Y* represents the biological response, *Bottom* stands for the minimum inhibition observed, *Top* is the maximum inhibition achieved and *X* is the concentration of the compound, on a molar scale, that affords each *Y* value.

Similarly, ΔTm obtained in the presence of NADH and NAD⁺ (0.6 mM), and phenazine-1-carboxylic acid (PCA) (1.0 mM) were employed to calculate the NADH-Tm, NAD⁺-Tm and the PCA-Tm curves. All measurements were carried out in triplicate and the sigmoid curves for each experiment were compared visually.

Compounds' affinity calculation by TSA

The effect of ligand's concentration (ranging from 3.12 to 200 µM) over the *PaPhzS* Tm (5 µM final concentration) was evaluated using the same parameters described in section (2.2.2). Next, the fraction of unfolded *PaPhzS* at 43 °C were employed to calculate the compounds Kd, using the DSFit software (default parameters), as described by Bai and co-workers⁵⁴. The ΔCp value (0.69) required for this calculation was predicted by hydrophobic surface area-based method available on <http://www.ibi.vu.nl/programs/bicepwww/>. Briefly, the heat capacity (*C*) was calculated at two temperatures: 25 °C (before PhzS unfolding [T1]) and 50 °C (after PhzS unfolding [T2]) using Equation (2).

$$C = 332.66 \pm 18.9 X (273.15 - T) + 52089 \pm 1353 \quad (2)$$

where *T* stands for temperature in Kelvin. Therefore T1 = 298.15 K, T2 = 323.15 K.

Compounds' affinity to covalently modified PaPhzS

PaPhzS (2 mg/mL) was incubated with fluorescein-5-isothiocyanate (FITC) dye (6 mg/mL) containing 50 mM HEPES (pH 8.0) for 2 h, at 25 °C. Then, the solution was loaded on a Hi-Trap HP desalting column (GE Healthcare), previously equilibrated with 50 mM HEPES buffer (pH 8) and 2 CV of the same buffer were injected. The absorbance of the collected fractions was monitored at 280 nm and 490 nm and those with a molar ratio ranging from 0.3 and 1.0⁵⁵ were employed for the K_d calculation experiments, as follows: The fluorescence of PaPhzS-FITC, at 25 °C, using in a real-time thermocycler (AppliedBiosystem7500) equipped with the FAN filter (excitation 498 nm and emission 530 nm wavelengths) for 10 min in the presence of different concentrations of each compound (3.12–100.0 μM). The Raw fluorescence data, recorded within the Applied Biosystems 7500 Software v2.0, was employed for non-linear regression analysis (three parameters) (Equation 1), as available in GraphPad Prism 8.0 software (GraphPadV[®] Software, San Diego, CA, USA, www.graphpad.com). All experiments were carried out in triplicate using 96-well PCR plate (PCR plates 96 well BioRad[®]), manually sealed with transparent capping strips (Flatcap strips BioRad[®]).

Results

Screening and K_d determination of thiazolidinone derivatives

TSA carried out at a single-concentration (50 μM) shows that approximately 60% of the compounds increase PhzS T_m value

more than 0.5 °C, however, this effect is statistically significant just for compounds **3**, **9**, **12**, **13**, **15**, **16**, **20**, **25**, **26**, **28**, **33**, **37** and **38** (Figure 3). Compounds with negative ΔT_m were not considered further. No compound substituted in N1 affords a significant change in PaPhzS T_m. Apart from compound **33**, the replacement of benzylidene ring by fused-rings (**30**–**35**) affords compounds that do not bind to PaPhzS. In order to reduce the number of false-positive hits identified in the initial screening, the effect of compounds **12**, **13**, **15**, **16**, **20**, **25**, **26**, **28**, **33**, **37** and **38** were also evaluated at different concentrations. Among these compounds, **12**, **13**, **15**, **16**, **20**, **28** and **33** showed a clear concentration-response profile (Figure 4 and Figure 1(S) – Supplementary material), which excludes a non-specific interaction to PaPhzS.

On the other hand, compounds **25** and **26** displayed a flat response in the concentration range investigated (3.12–100.0 μM) (Figure 1S – Supplementary material). Considering that **25** and **28** differ only at the substitution pattern at one position (2,3,4 OCH₃ vs. 1,3,4 OCH₃, respectively), it seems that substituents at *meta* play a crucial role towards PaPhzS binding. Compounds **37** and **38** showed a small variation in ΔT_m, along with poor fit (*r*² < 0.7) (Figure 1S – Supplementary material) and for that reason they were discarded.

Although some authors suggest that the compounds' affinity (K_d values) might be calculated directly from those curves with reasonable accuracy⁵⁶, there is some concern about the thermodynamic basis for this approach⁵⁷. Bai and co-workers devised an

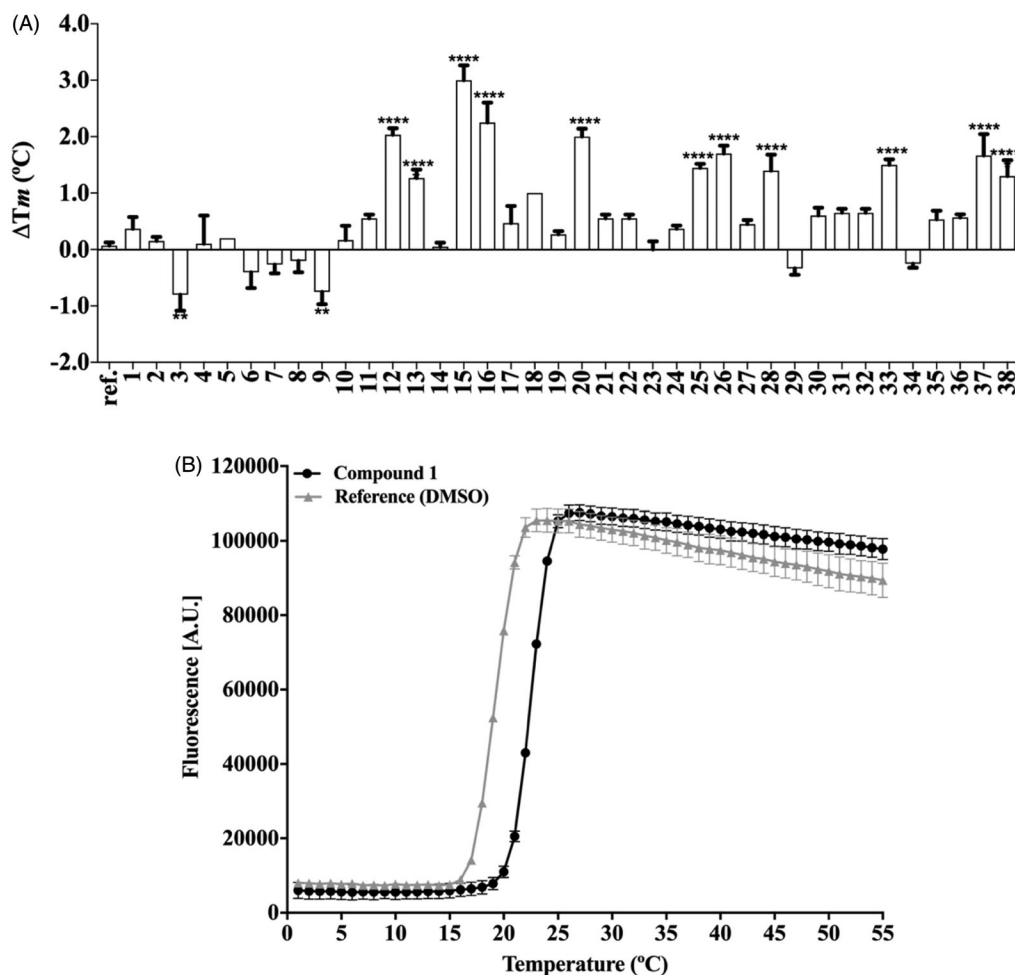


Figure 3. (A) Single-dose screening of thiazolidinone derivatives (50 μM) against PhzS from *P. aeruginosa*, by TSA. The ΔT_m values represents the mean ± SD of the changes in T_m of each compounds (***p* < .01, ****p* < .0001 compared with reference (DMSO)); (B) Raw data from TSA. All data represent the mean ± SD from three independent experiments.

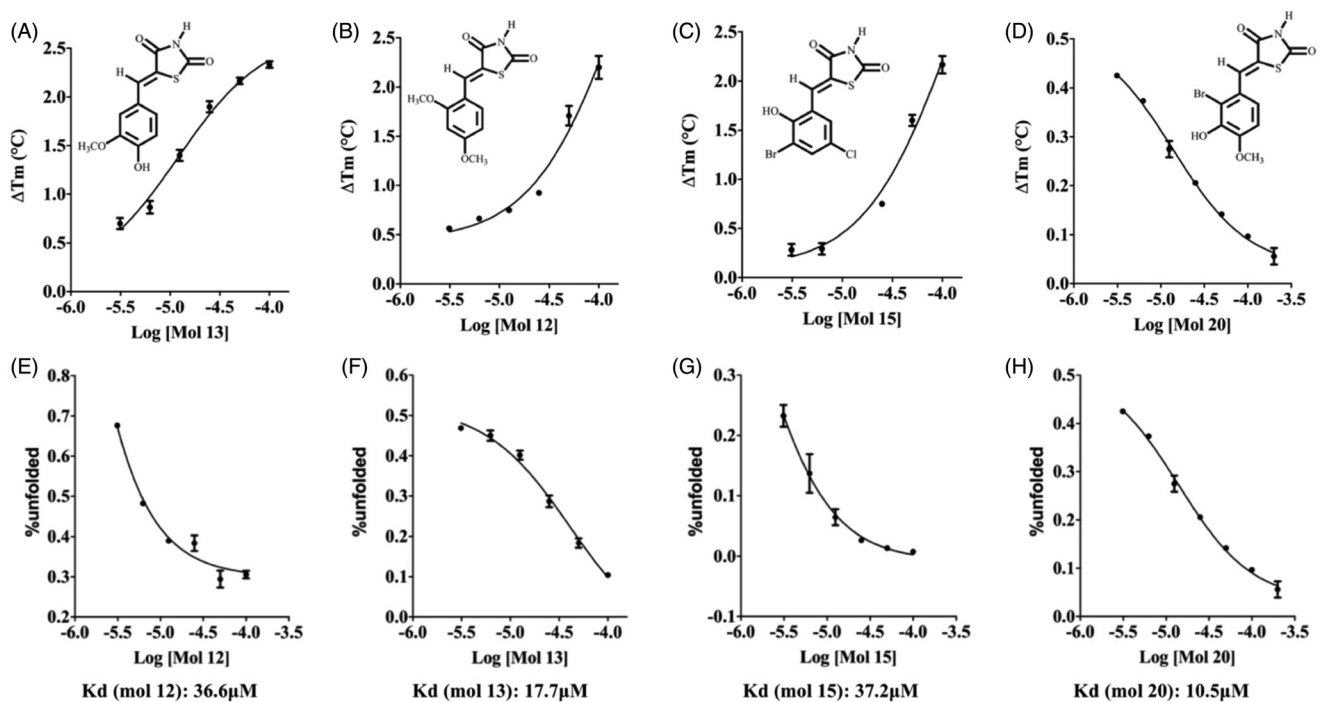


Figure 4. Effect of different concentrations of compounds 12, 13, 15 and 20 over the *PaPhzSTM* values (upper panel – A–D) and over the fraction on unfolded *PaPhzS* (lower panel – E–H) at 43°C. ΔT_m was calculated in comparison to DMSO (control) and Kd values were calculated using DSFit software. Plots were generated with GraphPad Prism v.8.0. All data represent the mean \pm SD from three independent experiments.

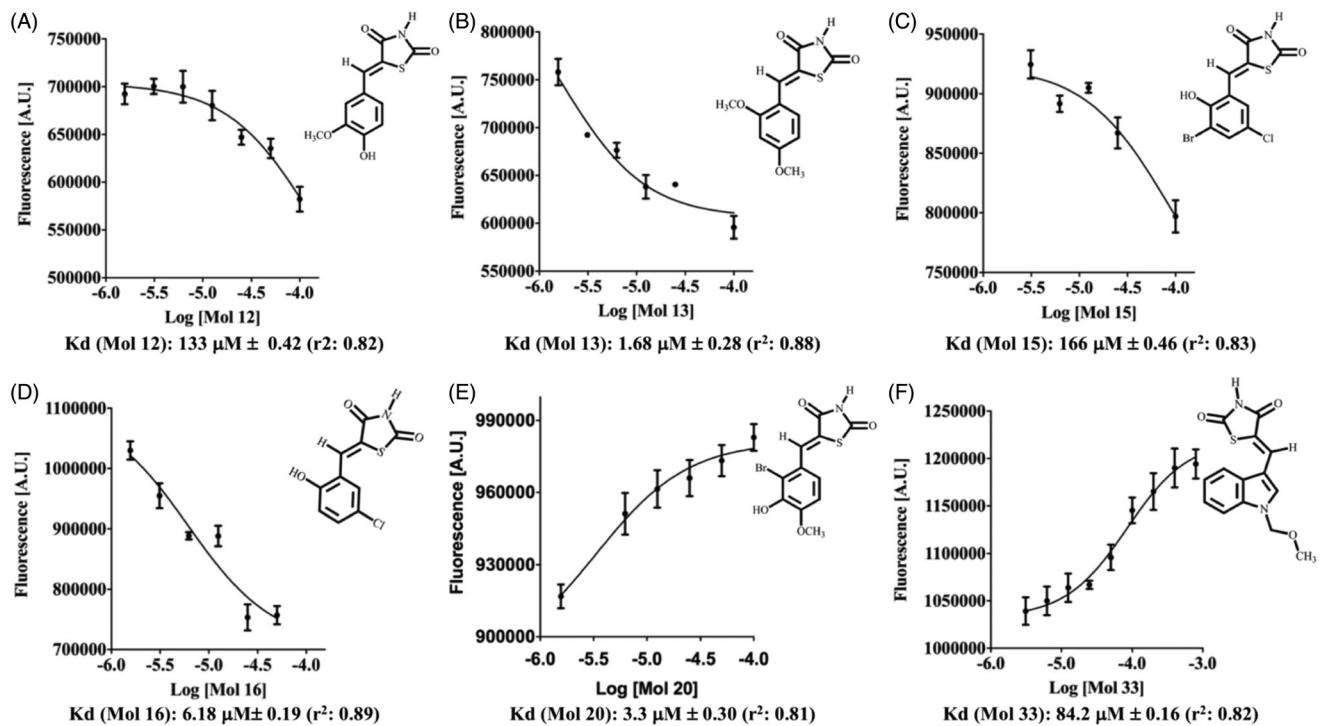


Figure 5. Effect of different concentrations of compounds 12, 13, 15, 16, 20 and 33 over the fluorescence signal (498 nm (excitation) and 530 nm (emission) wavelengths) of covalently labelled *PhzS* from *P. aeruginosa* (*PaPhzS*-FITC). Kd values were calculated by non-linear regression as available in GraphPad Prism v.8.0. All data represent the mean \pm SD from three independent experiments.

elegant workaround that limitation, which relies on the percentage of unfolded protein at a fixed temperature⁵⁴. Using this approach, the Kd values were calculated at 43°C, which is close to the *PaPhzS* T_m value in the absence of ligands (42°C), so that the fraction of folded and unfolded protein was close to 1.0.

According to Bai and co-workers (2019) Kd values close to the protein concentration (5 μ M) or lower should be taken with scepticism. However, only one compound had Kd value in this range (compound **16** - Kd = 4.2 μ M). The other compounds display affinity ranging from 10.5 – 50.5 μ M (compound **20** and compound **33**

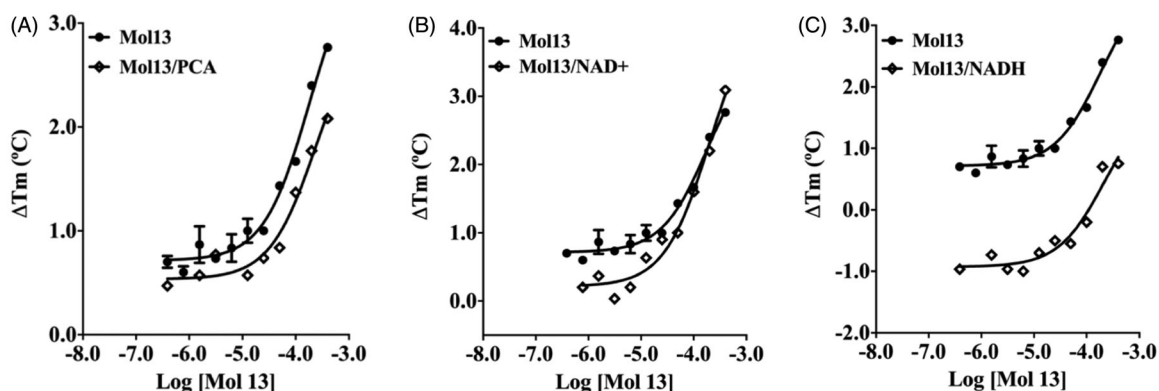


Figure 6. Thermal shift signatures of compound 13 in presence/absence of PCA (A) or NADH (B) or NAD⁺ (C). All data represent the mean \pm SD from three independent experiments.

Table 3. The binding affinity (Kd), ligand efficiency (LE)* and binding efficiency index (BEI)[#] of PaPhzS inhibitors.

DSFit software	DSFit			FITC		
	Kd (μ M)	LE	BEI	Kd (μ M)	LE	BEI
1A (previous hit)	9.3	0.21	11.0	18.0**	0.21	10.4
Mol 12	36.6	0.36	17.6	133 \pm 0.4	0.32	15.4
Mol 13	17.7	0.37	17.9	1.68 \pm 0.2	0.44	21.8
Mol 15	37.2	0.36	13.3	166 \pm 0.5	0.31	11.4
Mol 16	4.2	0.47	21.0	6.18 \pm 0.2	0.45	20.4
Mol 20	10.5	0.38	15.0	3.3 \pm 0.3	0.42	16.6
Mol 33	50.0	0.30	14.9	84.2 \pm 0.2	0.28	14.1

LE: 1.4 μ Kd/HA, where heavy (non-hydrogen) atoms [82].

[#]BEI: (μ Kd/MW) \times 1000, where MW is molecular weight (Da) [83].

**Kd value calculated by microscale thermophoresis [11].

respectively) (Figure 4 and Supplementary material Figure 3S). As these Kd values were obtained at a temperature higher than the physiologic one, we decided to employ an orthogonal assay to evaluate the compounds' affinity. In order to achieve this goal, PaPhzS was labelled with FITC and the effects of different concentration of each inhibitor on the covalently modified PaPhzS was monitored at 25 °C (Figure 5).

According to this assay, three compounds (**13**, **16** and **20**) are low micromolar ligands of PaPhzS, this result is in good agreement with previous results that also suggest these are the most promising compounds. The lower values of Kd obtained here might be a consequence of the reduced temperature employed in this assay. Although this assay also agrees that **12**, **15** and **33** have low affinity to PaPhzS their affinity for PaPhzS-FITC is even lower than calculated by DSFIT for PaPhzS. Since **13** and **28** differ by one OCH₃, it is tentative to assume that this moiety causes steric hindrance and abolishes the activity. In fact, no compound is substituted, simultaneously, at R3 and R4 is active. Moreover, comparison of compound **15** and **16** Kd values (166 μ M \pm 0.46 vs. 6.18 μ M \pm 0.19, respectively) and compound **19** (ΔT_m close to zero) supports the hypothesis that di-substitution at meta position is detrimental to the affinity.

Inhibition mode determination by TSA

Since the catalytic efficiency of PaPhzS to convert PCA to hydroxyphenazine is low and requires an excess of NADH (cofactor)²⁹, using kinetic assays to evaluate the mode of inhibition might be misleading. Considering that TSA has been employed as a suitable alternative to achieve this goal^{53,58–60}, we employed this approach to confirm that the most promising compound (**13**) binds to the cofactor binding site, through the analysis of its thermal shift

signature in the presence and absence of either the cofactor to the substrate (Figure 6).

Previously, we have shown that both the substrate and the cofactor cause a concentration-dependent decrease in PaPhzS's Tm value¹¹. Then, the ΔT_m curves of PaPhzS in the presence of a fixed concentration of either NADH (0.6 mM) or PCA (1.0 mM) are displaced south of the curve in their absence. Nevertheless, in the presence of either NADH or PCA, the curves are parallel to those seen in their absence. This profile is the opposite of the one described by Lea and co-workers,⁵³ but the overall analysis of the thermal signature holds: The parallel curves observed for compound **13** in the presence and absence of the PCA/NADH are compatible with the non-competitive mode of inhibition towards both the substrate and cofactor. This result might seem unexpected, once thiazolidinedione derivatives were expected to mimic the binding profile of the purine ring from NADH. One reasonable explanation is that FAD is readily reduced to FADH in the presence of NADH (Data not shown), and then NAD⁺ leaves the binding site, thus not affecting compound **13**'s affinity to PaPhzS. In order to support this hypothesis, we avoided the conformational shift that would expel NAD⁺ from its binding site, by performing the assay in the presence of NAD⁺. As anticipated, the curves get closer as the concentration of compound **13** increases, suggesting a competitive mode of inhibition to this compound and corroborating its binding profile to the cofactor binding site.

Discussion

The development of novel antibiotic drugs continues to be of utmost importance^{61,62}. However, the research and development of novel antibiotic drugs by the Big-Pharma industries has steadily declined in the last decades^{63,64}. There are some promising alternatives to deal with this issue^{65,66}. Among them, anti-virulence drug development relies on the hypothesis that is better to "live in peace with the enemy" than to kill it⁶⁷. One way to achieve this goal is by rendering the pathogenic bacteria harmless to the human host and assuming this process will put less evolutive pressure on the microorganism than the currently available drugs^{67–70}. Much effort has been put into the inhibition of pigmented virulence factors such as staphyloxanthin and pyocyanin^{71,72} but the approach is taken to their modulation is rather distinct. The first relies on the inhibition of druggable targets that are responsible for staphyloxanthin biosynthesis,^{73,74} whereas the second is focussed on the modulation of quorum sensing mechanisms that lie upstream the biosynthetic pathway that builds up this virulence factor^{75–78}.

According to Ni and co-workers (2019),⁷¹ targeting enzymes from the pyocyanin biosynthesis pathway is a valid and underexplored strategy. In accordance with this standpoint of view, it has been proposed that PaPhzS is a druggable target²⁸ and we have shown that thiazolidine-2,4-dione derivatives, bearing a dihydroquinazoline ring at the *para* position of the benzylidene ring, have a micromolar affinity to PhzS from *P. aeruginosa* and reduce pyocyanin production without a significant impact on the cell growth rate¹¹. The most promising compound (Figure 1(A)) might be employed for hit-to-lead optimisation efforts, but a careful analysis of its ligand efficiency argues otherwise. Molecular obesity has been one of the largest problems in drug development campaigns in the last decades^{79,80} and our initial effort to identify PaPhzS inhibitors seems to suffer from the same problem. In general, hits with LE > 0.30 have a higher success rate than those with lower LE, since this metric is highly correlated to high steric and electronic complementarity within the binding site. The low LE value for the previous hit (**1A**- LE = 0.21) suggests that some moieties are detrimental for it to fit into the binding site. This comes as no surprise, once molecular complexity is inversely related to LE⁸¹. Hence, an obvious alternative to increase LE is to strip the molecules from auxophoric groups and to focus on the chemical features that are essential for biological activity. Considering that previous work suggests the thiazolidine-2,4-dione ring mimics the cofactor binding profile, it was decided to evaluate whether N1-substituted compounds would bind to PaPhzS. The lack of activity seen in N1-substituted compounds (**1–7**) supports that the H-bonding capability of the nitrogen within the thiazolidine-2,4-dione ring is essential for PaPhzS binding. This result is in good agreement with the morphological similarity analysis carried out for dihydroquinazoline substituted thiazolidine-2,4-dione derivatives¹¹.

Next, the replacement of the central phenyl by fused heteroaromatic rings was probed. In contrast to N1 substitution, this strategy affords compounds that bind to PaPhzS with two-digit micromolar affinity (i.e. **33** PaPhzS-FITC-Kd = 84.2 μM and DSFit-Kd > 50). However, additional studies are required to settle once and for all if this is a promising lead-optimisation strategy since the substitution pattern on this ring remains unexplored. Following a more conservative approach, it was decided to replace dihydroquinazoline moiety with less-bulky substituents. This strategy afforded compounds with lower affinity, but with higher LE (**12** and **15**) than the initial hit (Figure 1(A)) (Table 3).

One might argue that LE provides an unfair advantage for fragment-like compounds such as those reported here, especially for compounds bearing halogen substituents. This concern is, at least partially, taken into account by the binding efficiency index⁸³, which considers the compounds' molecular weight instead of their heavy-atom count. When this metric is employed compound **15** displays the lowest BEI among the thiazolidine-2,4-dione derivatives reported in this work, but its value remains in the same range as the previous hit (BEI **1A** = 10.4 vs. **15** = 11.4). On the other hand, both assays show a significant improvement in the affinity and efficiency of **13** (Kd 1.68, LE = 0.45, BEI 21.79), **16** (Kd 6.18 LE = 0.46, BEI 20.42) and **20** (kd LE = 0.43, BEI 16.71). In an attempt to relate the structural changes in compounds with their putative interactions within the binding pocket, the difference in free energy of binding among those compounds ($\Delta\Delta G_{\text{binding}} = RT\ln(Kd^a/Kd^b)$ where Kd^a and Kd^b represent the affinity of two compounds being compared, $R=8.31$ J/Kmol and $T=298.15$ K) can be calculated. $\Delta\Delta G_{\text{binding}}$ between compounds **12** and **13**, using PaPhzS-FITC-Kd values, yields a difference that is compatible with an H-bond (2.6 Kcal/mol). Similar values are seen for the

comparison between compounds **13** and **15** (2.7 Kcal/mol), compounds **12** and **20** (2.2 Kcal/mol) and compounds **15** and **20** (2.3 Kcal/mol). These values support the importance of H-bonding ability to potency. This feature might be correlated with the keto-enol tautomerism as well as the planarity between the 5-arylidene and the thiazolidine-2,4-dione moieties, which are affected by electron-donating/accepting substituents decorating the ring⁸⁴. In fact, *para* electron-accepting groups that stabilise the keto-form only afford inactive compounds (**8–11**), and except for compound **20**, the same can be stated for substituents in the *ortho* position (either R1 or R5). On the other hand, steric restraints also play a key role for thiazolidine-2,4-dione binding affinity, as observed for *meta* disubstituted compounds: **19** and **25** are inactive, whereas **15** shows reduced affinity in comparison to **13**, **16** or **20**, all of which have only one substitution at *meta* position.

When molecular simplification is carried out, conformational flexibility may cause the novel compounds to adopt new bioactive conformations or even explore small binding clefts that were inaccessible at first. The results provided by the mode of inhibition studies suggest this is not the case for the compounds reported in this work and suggests the same structure-activity relationships hold for the whole series. Last but not least, careful analysis of TSA raw curves (Figure 2S – Supplementary material) hint that these compounds do not behave as classical PAINS⁸⁵, which reinforces their usefulness as a promising scaffold to design novel mechanism-based inhibitors of PaPhzS.

Conclusion

One approach to overcome the dilemma relies on bacterial virulence modulation. Although pyocyanin is a virulence factor from *Pseudomonas aeruginosa* employed as an end-point in most anti-virulence drug development projects, the enzymes responsible for its biosynthesis remain largely unexplored as potential therapeutic targets. The results described here show that unsubstituted N1 at the thiazolidine-2,4-dione ring is essential for PaPhzS inhibition and that molecular simplification of (E)-5-(4-((4-oxo-3-phenyl-3,4-dihydroquinazolin-2-yl)methoxy)benzylidene)thiazolidine-2,4-dione affords improved lead compounds that retain the original mode of inhibition (competitive to NAD⁺). Moreover, steric clashes due to simultaneous substitution at both meta positions are detrimental to 5-arylidene-thiazolidine-2,4-dione derivatives affinity. However, there seems to be some plasticity within PaPhzS binding site, since the replacement of benzyl ring by indole substituted ring does not abolish the affinity. Taken together, this information paves the way to develop the third round of PaPhzS inhibitors with improved potency.

Disclosure statement

The authors declare that there are no conflicts of interest. The founding sponsors had no role in the design of the study; in the collection, analysis, or interpretation of data; in the writing of the manuscript, nor in the decision to publish the results.

Funding

The authors acknowledge the support provided by CNPq [310138/2017-5 and 421304/2018-9], CAPES [TQF's fellowship 88881.134191/2016-01] and Dr. James Parsons [Maryland University – USA] for providing the plasmids with PhzS from *P. aeruginosa*.

ORCID

Marcelo Santos Castilho  <http://orcid.org/0000-0002-9563-5679>

References

1. Tomašić T, Peterlin Mašič L. Rhodanine as a scaffold in drug discovery: a critical review of its biological activities and mechanisms of target modulation. *Expert Opin Drug Discov* 2012;7:549–60.
2. Tripathi AC, Gupta SJ, Fatima GN, et al. 4-Thiazolidinones: the advances continue... *Eur J Med Chem* 2014;72:52–77.
3. Mendgen T, Steuer C, Klein CD. Privileged scaffolds or promiscuous binders: a comparative study on rhodanines and related heterocycles in medicinal chemistry. *J Med Chem* 2012;55:743–53.
4. Welsch ME, Snyder SA, Stockwell BR. Privileged scaffolds for library design and drug discovery. *Curr Opin Chem Biol* 2010;14:347–61.
5. Willson TM, Cobb JE, Cowan DJ, et al. The structure-activity relationship between peroxisome proliferator-activated receptor gamma agonism and the antihyperglycemic activity of thiazolidinediones. *J Med Chem* 1996;39:665–8.
6. Ramirez MA, Borja NL. Epalrestat: an aldose reductase inhibitor for the treatment of diabetic neuropathy. *Pharmacotherapy* 2008;11:231–5.
7. Leite FHA, Santiago PD, Froes TQ, et al. Structure-guided discovery of thiazolidine-2,4-dione derivatives as a novel class of *Leishmania major* pteridine reductase 1 inhibitors. *Eur J Med Chem* 2016;123:639–48.
8. Neri FSM, Costa JD, Froes TQ, et al. Antileishmanial activity evaluation of thiazolidine-2,4-dione against *Leishmania infantum* and *Leishmania braziliensis*. *Parasitol Res* 2020;119:2263–74.
9. Bhattarai BR, Kafle B, Hwang JS, et al. Thiazolidinedione derivatives as PTP1B inhibitors with antihyperglycemic and antiobesity effects. *Bioorganic Med Chem. Lett* 2009;19:6161–5.
10. Bhat BA, Ponnala S, Sahu DP, et al. Synthesis and antihyperglycemic activity profiles of novel thiazolidinedione derivatives. *Bioorg Med Chem* 2004;12:5857–64.
11. Froes TQ, Guido RVC, Metwally K, Castilho MS. A novel scaffold to fight *P. aeruginosa* pyocyanin production: early-steps to novel anti-virulence drugs. *Future Med Chem* 2020;16:104155.
12. Access to Medicine Foundation. Antimicrobial Resistance Benchmark 2018. (2018). Available from: https://access-to-medicine-foundation.org/media/uploads/downloads/5c46f0d1cbefe_Antimicrobial-Resistance-Benchmark-2018.pdf
13. Centers for Disease Control and Prevention. Antibiotic Use in the United States. 2017: Progress and Opportunities. Available from: <https://www.cdc.gov/antibiotic-use/stewardship-report/pdf/stewardship-report.pdf>
14. O'Neill J. Securing new drugs for future generations: the pipeline of antibiotics – review on antimicrobial resistance. *Rev Antimicrob Resist* 2016;44:1–44.
15. Ventola CL. The antibiotic resistance crisis: part 1: causes and threats. *P T A Peer-Reviewed J Formul Manag* 2015;40:277–83.
16. World Health Organization. Global action plan on antimicrobial resistance. (2015). Available from: https://apps.who.int/iris/bitstream/handle/10665/193736/9789241509763_eng.pdf?sequence=1
17. Ali J, Rafiq QA, Ratcliffe E. Antimicrobial resistance mechanisms and potential synthetic treatments. *Futur Sci OA* 2018;4:FSO290.
18. Clatworthy AE, Pierson E, Hung DT. Targeting virulence: a new paradigm for antimicrobial therapy. *Nat Chem Biol* 2007;3:541–8.
19. Rasko DA, Sperandio V. Anti-virulence strategies to combat bacteria-mediated disease. *Nat Rev Drug Discov* 2010;9:117–28.
20. Shoham M, Greenberg M. Preventing the spread of infectious diseases: antivirulence versus antibiotics. *Future Microbiol* 2017;12:365–8.
21. Forezi LSM, Froes TQ, Cardoso MFC, et al. Synthesis and biological evaluation of coumarins derivatives as potential inhibitors of the production of *Pseudomonas aeruginosa* virulence factor pyocyanin. *Curr Top Med Chem* 2018;18:149–56.
22. Müh U, Schuster M, Heim R, et al. Novel *Pseudomonas aeruginosa* quorum-sensing inhibitors identified in an ultra-high-throughput screen. *Antimicrob Agents Chemother* 2006;50:3674–9.
23. Paczkowski JE, Mukherjee S, McCready AR, et al. Flavonoids suppress *Pseudomonas aeruginosa* virulence through allosteric inhibition of quorum-sensing receptors. *J Biol Chem* 2017;292:4064–76.
24. Defoirdt T. Quorum-sensing systems as targets for antivirulence therapy. *Trends Microbiol* 2018;26:313–28.
25. Fong J, Mortensen KT, Nørskov A, et al. Itaconimides as novel quorum sensing inhibitors of *Pseudomonas aeruginosa*. *Front Cell Infect Microbiol* 2018;8:443–11.
26. European Centre for Disease Prevention and Control. Surveillance of antimicrobial resistance in Europe Annual report of the European Antimicrobial Resistance Surveillance Network (EARS-Net) 2017.
27. Lau GW, Ran H, Kong F, et al. *Pseudomonas aeruginosa* pyocyanin is critical for lung infection in mice. *Infect Immun* 2004;72:4275–8.
28. Froes TQ, Baldini RL, Vajda S, Castilho MS. Structure-based druggability assessment of anti-virulence targets from *Pseudomonas aeruginosa*. *Curr Protein Pept Sci* 2019;20:1189–203.
29. Greenhagen BT, Shi K, Robinson H, et al. Crystal structure of the pyocyanin biosynthetic protein PhzS. *Biochemistry* 2008;47:5281–9.
30. Blankenfeldt W, Parsons JF. The structural biology of phenazine biosynthesis. *Curr Opin Struct Biol* 2014;29:26–33.
31. Romagnoli R, Baraldi PG, Salvador MK, et al. Anticancer activity of novel hybrid molecules containing 5-benzylidene thiazolidine-2,4-dione. *Eur J Med Chem* 2013;63:544–57.
32. Barros CD, Amato AA, Oliveira T. d, et al. Synthesis and anti-inflammatory activity of new arylidene-thiazolidine-2,4-diones as PPARgamma ligands. *Bioorg Med Chem* 2010;18:3805–11.
33. Ates-Alagoz Z, Altanlar N, Buyukbingol E. Synthesis of 4-substituted 2-(4-Methylpiperazino) pyrimidines and quinazoline analogs as serotonin 5-HT 2A receptor ligands. *J Heterocycl Chem* 2009;46:1259–65.
34. Tuncbilek M, Altanlar N. Synthesis of new 3-(substituted phenacyl)-5-[3'-(4H-4-oxo-1-benzopyran-2-yl)-benzylidene]-2,4-thiazolidinediones and their antimicrobial activity. *Arch Pharm* 2006;339:213–6.
35. Alhameed RA, Almarhoon Z, Bukhari SI, et al. Synthesis and antimicrobial activity of a new series of thiazolidine-2,4-

- diones carboxamide and amino acid derivatives. *Molecules* 2019;25:105–17.
36. Tahlan S, Verma PK. Synthesis, SAR and *in vitro* therapeutic potentials of thiazolidine-2,4-diones. *Chem Cent J* 2018;12:1–11.
 37. Liu Y, Li R, Xing Y. A simple, efficient and green procedure for Knoevenagel condensation in hydroxy-functionalized ionic liquids. *Heterocycles* 2015;91:1385–97.
 38. De Paiva RKC, Da Silva JF, Moreira HA, et al. Synthesis, antimicrobial activity and structure-activity relationship of some 5-arylidene-thiazolidine-2,4-dione derivatives. *J Braz Chem Soc* 2018;30:164–72.
 39. Khan FAK, Patil RH, Shinde DB, Sangshetti JN. Design and synthesis of 4'-((5-benzylidene-2,4-dioxothiazolidin-3-yl)methyl)biphenyl-2-carbonitrile analogs as bacterial peptide deformylase inhibitors. *Chem Biol Drug Des* 2016;88:938–44.
 40. Azad L, Ghazvini M, Sanaeishoar H, Yavari I. Synthesis of functionalized 1,2-dihydroisoquinolines via one-pot reactions of isoquinoline, alkyl propiolate, and thiazolidin-2,4-dione. *J Chem Res* 2019;43:457–60.
 41. Da Silva IM, Da Silva Filho J, Santiago P, et al. Synthesis and antimicrobial activities of 5-arylidene-thiazolidine-2,4-dione derivatives. *Biomed Res Int* 2014;2014:316082.
 42. Zhang Y, Zhou Z. A solvent-free protocol for the green synthesis of 5-arylidene-2,4-thiazolidinediones using ethylenediamine diacetate as catalyst. *Org Chem Int* 2012;2012:1–5.
 43. Sharma H, Lather V, Grewal AS, Pandita D. Synthesis, anti-inflammatory activity and docking studies of some newer 1,3-thiazolidine-2,4-dione derivatives as dual inhibitors of PDE4 and PDE7. *Curr Comput Aided Drug Des* 2019;15:225–34.
 44. Mohanty S, Roy AK, Sandeep Reddy G, et al. Knoevenagel condensation of aromatic bisulfite adducts with 2,4-thiazolidinedione in the presence of Lewis acid catalysts. *Tetrahedron Lett* 2015;56:2564–7.
 45. Palkar M, Jalalpure S, Rane R, et al. novel series of coumarinyl substituted-thiazolidin-2,4-dione analogs as anticancer agents: design, synthesis, spectral studies and cytotoxicity evaluation. *Anticancer Agents Med Chem* 2015;15:970–9.
 46. Kaarsholm B, Christian N, Olsen B. Preparation of novel ligands for the HisB10 Zn²⁺ sites of the R-state insulin hexamer and their use in pharmaceutical preparations comprising insulin. *PCT Int. Appl.* 2006;3–7:WO 2006082245 A1 20060810.
 47. Chandrappa S, Vinaya K, Prasanna DS, Rangappa KS. Mild and highly efficient method for the synthesis of arylidene-thiazolidinone analogues. *Proc Indian Natl Sci Acad* 2011;77:343–9.
 48. Sato S, Shirakawa S, Tatsui A, et al. Thiazolidine derivatives as chymase inhibitors and prophylactic and therapeutic drugs containing them for cardiovascular diseases. *Jpn Kokai Tokkyo Koho* 2000; JP 2000095770 A 20000404.
 49. Maccari R, Ottanà R, Curinga C, et al. Structure-activity relationships and molecular modelling of 5-arylidene-2,4-thiazolidinediones active as aldose reductase inhibitors. *Bioorg Med Chem* 2005;13:2809–23.
 50. Libermann D, Himbert J. HL. La thiazolidione, point de départ d'une synthèse des acides thiopyruviques et thio-glyoxiliques substituées. *Bull Soc Chim Fr* 1948;11–12:1120–4.
 51. Albuquerque JF, Azevedo LC, Galdino SL, Chantegrel J, et al. Synthesis and structural study of 5-arylidene thiazolidine-2,4-diones and 3-substituted-4-thio-imidazolidine-2-ones. *Ann Pharm Fr* 1995;53:209–14.
 52. Grøftehaug MK, Hajizadeh NR, Swann MJ, Pohl E. Protein-ligand interactions investigated by thermal shift assays (TSA) and dual polarization interferometry (DPI). *Acta Crystallogr D Biol Crystallogr* 2015;71:36–44.
 53. Lea WA, Simeonov A. Differential scanning fluorometry signatures as indicators of enzyme inhibitor mode of action: case study of glutathione s-transferase. *PLOS One* 2012;7:e36219.
 54. Bai N, Roder H, Dickson A, Karanicolas J. Isothermal analysis of thermofluor data can readily provide quantitative binding affinities. *Sci Rep* 2019;9:2650–15.
 55. The TH, Feltkamp TEW. Conjugation of fluorescein isothiocyanate to antibodies I. Experiments on the conditions of conjugation. *Immunology* 1970;18:865–73.
 56. Vivoli M, Novak HR, Littlechild JA, Harmer NJ. Determination of protein-ligand interactions using differential scanning fluorimetry. *J Vis Exp* 2014;91:1–13.
 57. Cimperman P, Baranauskienė L, Jachimovičiūtė S, et al. A quantitative model of thermal stabilization and destabilization of proteins by ligands. *Biophys J* 2008;95:3222–31.
 58. Niesen FH, Schultz L, Jadhav A, et al. High-affinity inhibitors of human NAD⁺-dependent 15-hydroxyprostaglandin dehydrogenase: mechanisms of inhibition and structure-activity relationships. *PLoS One* 2010;5:e13719.
 59. Auld DS, Lovell S, Thorne N, et al. Molecular basis for the high-affinity binding and stabilization of firefly luciferase by PTC124. *Proc Natl Acad Sci U S A* 2010;107:4878–83.
 60. Simeonov A. Recent developments in the use of differential scanning fluorimetry in protein and small molecule discovery and characterization. *Expert Opin Drug Discov* 2013;8:1–20.
 61. World Health Organization. . Antibacterial agents in clinical development: an analysis of the antibacterial clinical development pipeline. 2019. Available from: <https://apps.who.int/iris/bitstream/handle/10665/330420/9789240000193-eng.pdf>
 62. Renwick MJ, Brogan DM, Mossialos E. A systematic review and critical assessment of incentive strategies for discovery and development of novel antibiotics. *J Antibiot* 2016;69:73–88.
 63. Renwick M, Mossialos E. What are the economic barriers of antibiotic R&D and how can we overcome them? *Expert Opin Drug Discov* 2018;13:889–92.
 64. Dheman N, Mahoney N, Cox EM, et al. An analysis of antibacterial drug development trends in the United States, 1980–2019. *Clin Infect Dis* 2020;72:1–7.
 65. Hoffman PS. Antibacterial discovery: 21st century challenges. *Antibiotics* 2020;9:1–10.
 66. Calvert MB, Jumde VR, Titz A. Pathoblockers or antivirulence drugs as a new option for the treatment of bacterial infections. *Beilstein J Org Chem* 2018;14:2607–17.
 67. Dickey SW, Cheung GYC, Otto M. Different drugs for bad bugs: antivirulence strategies in the age of antibiotic resistance. *Nat Rev Drug Discov* 2017;16:457–71.
 68. Inglis RF, Brown SP, Buckling A. Spite versus cheats: competition among social strategies shapes virulence. *Pseudomonas Aeruginosa. Evolution* 2012;66:3472–84.
 69. El-halfawy OM, Czarny TL, Flannagan RS, et al. Discovery of an antivirulence compound that reverses β -lactam resistance in MRSA. *Nat Chem Biol* 2020;16:143–9.

70. Lindsay RJ, Kershaw MJ, Pawlowska BJ, et al. Harboring public good mutants within a pathogen population can increase both fitness and virulence. *Elife* 2016;5:1–25.
71. Ni S, Li B, Xu Y, et al. Targeting virulence factors as an antimicrobial approach: pigment inhibitors. *Med Res Rev* 2020;40:293–338.
72. Liu GY, Nizet V. Color me bad: microbial pigments as virulence factors. *Trends Microbiol* 2009;17:406–13.
73. Song Y, Liu CI, Lin FY, et al. Inhibition of staphyloxanthin virulence factor biosynthesis in *Staphylococcus aureus*: *in vitro*, *in vivo*, and crystallographic results. *J Med Chem* 2009;52:3869–80.
74. Wang Y, Chen F, Di H, et al. Discovery of potent benzofuran-derived diapophytoene desaturase (CrtN) inhibitors with enhanced oral bioavailability for the treatment of methicillin-resistant *Staphylococcus aureus* (MRSA) infections. *J Med Chem* 2016;59:3215–30.
75. Miller LC, O'Loughlin CT, Zhang Z, et al. Development of potent inhibitors of pyocyanin production in *Pseudomonas aeruginosa*. *J Med Chem* 2015;58:1298–306.
76. Wang M, Zhao L, Wu H, et al. Cladodione is a potential quorum sensing inhibitor. *Mar Drugs* 2020;18:205–14.
77. Malešević M, Di LF, Filipić B, et al. *Pseudomonas aeruginosa* quorum sensing inhibition by clinical isolate *Delftia tsuruhatensis* 11304: involvement of N-octadecanoylhomoserine lactones. *Sci Rep* 2019;9:1–13.
78. Kitao T, Lepine F, Babloui S, et al. Cross-molecular insights into function and competitive inhibition of *Pseudomonas aeruginosa* multiple virulence factor regulator. *MBio* 2018;9:1–13.
79. Polanski J, Bogocz J, Tkocz A. The analysis of the market success of FDA approvals by probing top 100 bestselling drugs. *J Comput Aided Mol Des* 2016;30:381–9.
80. Elsebaei MM, Abutaleb NS, Mahgoub AA, et al. Phenylthiazoles with nitrogenous side chain: an approach to overcome molecular obesity. *Eur J Med Chem* 2019;182:111593.
81. Hann MM, Leach AR, Harper G. Molecular complexity and its impact on the probability of finding leads for drug discovery. *J Chem Inf Comput Sci* 2001;41:856–64.
82. Hopkins AL, Groom CR, Alex A. Ligand efficiency: a useful metric for lead selection. *Drug Discov Today* 2004;9:430–1.
83. Abad-Zapatero C, Metz JT. Ligand efficiency indices as guideposts for drug discovery. *Drug Discov Today* 2005;10:464–9.
84. Tri N, Marinkovi A, Ran M. Spectrochimica acta part A: molecular and biomolecular spectroscopy substituent and solvent effects on intramolecular charge transfer of. *Spectrochim Acta Part A* 2012;86:500–7.
85. Redhead M, Satchell R, Swift D, et al. A combinatorial biophysical approach; FTSA and SPR for identifying small molecule ligands and PAINs. *Anal Biochem* 2015;479:63–73.